Universidad de Valladolid

ESCUELA DE INGENIERÍAS INDUSTRIALES

MÁSTER EN INGENIERÍA AMBIENTAL

MASTER EN INGENIERÍA AMBIENTAL

ESCUELA DE INGENIERÍAS INDUSTRIALES

UNIVERSIDAD DE VALLADOLID

TRABAJO FIN DE MÁSTER

Detection of ammonia toxicity in microalgae by chlorophyll fluorescence

Autor: Yuto Izawa

Tutor: Masatoshi Kishi

Raúl Muñoz

Valladolid, Julio, 2025

Abstract

To improve the specificity and accuracy of ammonia detection in *Chlorella vulgaris* under high temperature, high light, and ammonia stress conditions, fast chlorophyll *a* fluorescence induction (OJIP) curve was measured using varying saturation pulse intensities and analyzed through multivariable statistical methods. The OJIP curve shapes alone showed limited discriminative power, as the fluorescence signals at the J and I phases were similar across the three stress conditions. Quantitative evaluation using OJIP parameters revealed relatively high correlations between ammonia concentration and specific parameters such as V_L and V_K ($R^2 = 0.683$ and 0.642, respectively). Moreover, the application of multivariable analysis using a broader set of OJIP parameters significantly improved both prediction accuracy and correlation (0.84 and 0.92, respectively). Additionally, the use of different saturation pulse intensities enabled clearer detection of the L- and K-bands, enhancing the reliability of these fluorescence features. These precisely captured parameters contributed to the improved performance of ammonia detection (prediction accuracy and correlation were 0.91 and 0.96). On the other hand, the model generated at different saturation pulse intensity largely misestimated ammonia concentration.

Acknowledgment

I would like to express my heartfelt gratitude to my supervisor, Prof. Dr. Raúl Muñoz Torre, and to Dr. Masatoshi Kishi for their invaluable guidance and support throughout my Master's studies. I am especially grateful for their academic insight, thoughtful encouragement, and the many opportunities they provided during my time in the laboratory. My sincere appreciation also goes to my supervisor in Japan, Prof. Dr. Tatsuki Toda (Soka University), for enabling me to participate in the double degree Master's program at the Universidad de Valladolid.

I would like to thank all the professors at the Escuela de Ingenierías Industriales, Universidad de Valladolid, as well as the members of the Institute of Sustainable Processes, for their continuous support and encouragement throughout my academic and personal life in Spain. Lastly, I am deeply thankful to the administrative staff at both the Universidad de Valladolid and Soka University for their kind and efficient support, which made it possible for me to pursue my studies in Spain.

Index

1. Introduction

1.1. Ammonia inhibition of wastewater treatment

Microalgae have been utilized for a tertiary treatment process of various types of wastewater, domestic wastewater (Sawayama et al., 1992), livestock wastes (Lincoln et al., 1986), and urban wastewater (Gentil et al., 2017), due to their ability to remove nutrients such as nitrogen and phosphorus, while simultaneously producing valuable compounds such as proteins, fatty acids, and pigments.

However, these wastewaters contain high concentrations of ammonia. Livestock wastewater, such as piggery effluent, contains ammonia at concentrations ranging from 120 to 2945 mg L^{-1} (Lee et al., 2021). In contrast, the EC_{50} (the concentration at which algal growth is reduced by 50%) for ammonia in microalgae is relatively low, ranging from 0.05 to 34 mg L^{-1} (Collos and Harrison, 2014). Therefore, various strategies have been employed to mitigate ammonia toxicity in algal-based wastewater treatment systems. For example, Marchão et al. (2018) demonstrated that diluting brewery wastewater to a dilution rate of 0.26 d^{-1} maximized the biomass productivity of *Scenedesmus obliquus*. Sutherland (2022) reported that the addition of glucose alleviated ammonia toxicity in food-waste concentrate wastewater. These findings highlight the importance of controlling ammonia concentration and its inhibitory effects when using microalgae for wastewater treatment. Accordingly, the management of ammonia concentration has emerged as a critical and extensively studied aspect in the context of wastewater treatment.

1.2. OJIP measurement as ammonia monitoring

OJIP measurement is widely used to evaluate performance of photosynthetic system, mainly PSII. The OJIP curve is a change of chlorophyll fluorescence intensity over microseconds to a second obtained by exposing photosynthetic systems to strong light, characterized by multiple peaks (O, J, I and P) that reflect different stages of the photochemical process (Fig. 1). As each peak corresponds to the electron transfer rate at a specific step within the photosynthetic electron transport, the overall shape of the OJIP curve varies according to the specific inhibitory conditions applied. This method is easy, fast, and supplies a lot of information about function of photosynthetic system of PSII. From this, OJIP measurement is used for detection of some inhibition factors such as temperature, high light, drought, salinity and ammonia stress (Thach et al., 2007; Wang et al., 2011, Koller et al., 2013; Markou et al, 2016). As these facts, OJIP curve can be the tool to monitor ammonia inhibition of microalgae in wastewater treatment. In fact, detection of other inhibition factors of microalgae using OJIP curve has been studied in recent years. For example, Gan et al. (2023) reported that six typical toxic pollutants (Cd, atrazine, 1,4-benzoquinone, 1,4-dichlorobenzene, chloroacetic acid, and trichloroacetonitrile) characteristically changed OJIP curve by different inhibition mechanisms in experiments that used *Chlorella pyrenoidosa*. In addition, using OJIP fluorescence intensity, Duarte et al. (2021) successfully distinguished various heavy metal inhibitors (Cr, Cu, Zn, and Hg) with a fairly high accuracy from 60% to 100%. They achieved such high accuracy discrimination by raw OJIP datasets with multivariable statistical analysis method. These findings suggest that OJIP can be an effective tool for detection and discrimination of ammonia inhibition from other inhibitions.

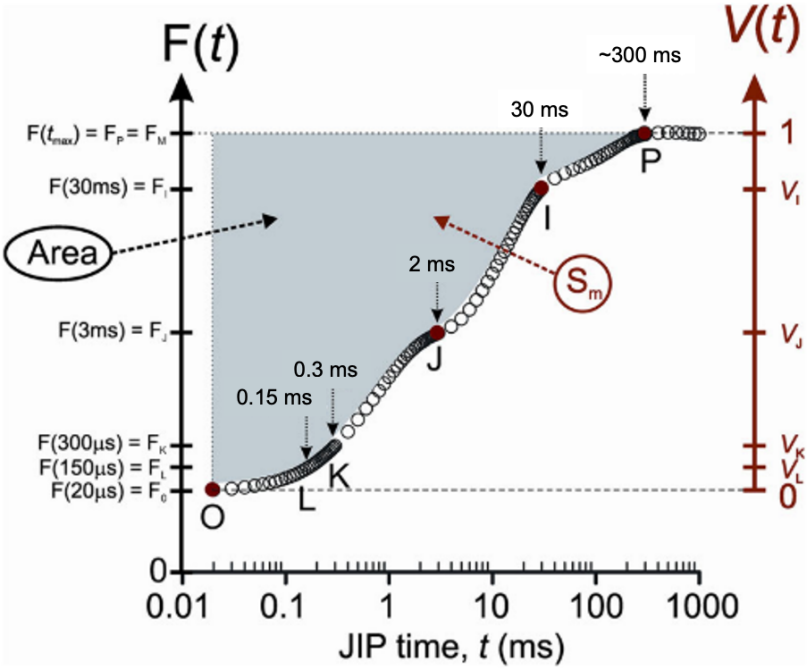

Fig. 1. Modified OJIP curve from Kalaji et al., 2014

1.3. Challenges of ammonia management in outdoor wastewater treatment

Although OJIP curve has been used to detect and distinguish various inhibition factors, knowledge of distinguishing ammonia inhibition from environmental inhibition factors such as heat and high light stress is limited. However, since most wastewater treatment plants using microalgae are located outdoors, high temperature and high irradiation can be inhibiting factors for microalgae. Under these conditions, specific ammonia inhibition distinction is necessary for ammonia management.

Previous studies reported that both heat and ammonia stress can harm the oxygen-evolving complex (OEC) of PSII (Strasser, 1997; Georgieva et al., 2000), suggesting these two inhibitors to photosystem may be difficult to distinguish. Furthermore, ammonia toxicity is enhanced under high light intensity condition (Markou et al., 2016). These facts indicate that temperature, high irradiation and ammonia stresses have the possibility to be complex inhibitors for microalgae in outdoor conditions. Hence, specific ammonia detection is required for ammonia management. In addition to that, the accuracy of detection is also necessary. As mentioned above, wastewater contains a large amount of ammonia, which can exceed limit of microalgal ammonia tolerance, and microalgae may be heavily damaged. To avoid such irreversible damage, ammonia management should be operated based on accurate ammonia inhibition detection.

1.4. Multivariable analysis for the detection of ammonia

Although inhibitory factors alter the OJIP curve, it also varies depending on the intensity of the inhibition, indicating that distinguishing specific inhibitory causes based solely on the

OJIP curve is difficult. Therefore, by identifying OJIP parameters that are particularly sensitive to specific inhibitory factors, it may be possible to specifically detect ammonia-induced inhibition. Conventional statistical methods are not an effective tool to analyze large amounts of data like OJIP datasets. In contrast, multivariable analysis provides an efficient tool for OJIP data analysis. For example, Duarte et al. (2021) successfully applied multivariable statistical analysis to OJIP parameters, achieving high-accuracy detection of heavy metal inhibitors. In addition, Kishi conducted experiments using *Chlorella vulgaris* Beijerinck SAG 211-11b, *Acutodesmus obliquus* (Turpin) Hegewald et Hanagata SAG 276-3a, and the cyanobacterium *Arthrospira platensis* (Nordstedt) Gomont SAG 21.99. By applying Lasso regression analysis, a type of multivariable analysis, to the OJIP data obtained from these microalgae that were exposed to ammonia stress, Kishi successfully predicted ammonia concentrations with a relatively high probability exceeding 60% (unpublished data). These findings suggest that processing OJIP data through multivariable analysis enables the selective detection of ammonia stress from other inhibitory factors.

1.5. Saturation pulse for accurate ammonia prediction

Since the accuracy of multivariable analysis is highly dependent on the quality of the raw OJIP data obtained, precise measurement of OJIP curves is essential for improving the accuracy of ammonia detection. A research conducted at the Institute of Sustainable Processes observed that the OJIP transients of microalgae treated with NO_3 and NH_4 changed depending on the intensity of the saturating pulse used for measurement of OJIP curve (unpublished). When measured under low saturating light (750 µmol m^{-2} s^{-1}), no difference was observed between the NO_3 and NH_4 treatments. In contrast, when measured under high saturating light (14000 µmol m^{-2} s^{-1}), the OJIP curves differed between the two treatments. This is likely due to either enhanced inhibition in the NH_4-treated samples under high saturation pulse intensity or increased fluorescence intensity, making the differences more detectable. In either case, adjusting the saturating light intensity may contribute to more accurate measurement of OJIP, then improve the detection of ammonia-induced inhibition.

2. Objectives

The aim of this study was to distinguish ammonia inhibition for microalgae from environmental inhibition factors, temperature, and high light stress, and improve the accuracy of detecting ammonia inhibition as an ammonia monitoring tool. This study focused on the detection of specific ammonia inhibition and the improvement of the ammonia detection accuracy by applying multivariable analysis and saturation pulse intensity changing, respectively. This study's results can contribute to ammonia management in wastewater treatment plants using microalgae outdoors.

3. Materials and methods

3.1. Algal strains, culture media and cultivation conditions

The green alga *Chlorella vulgaris* Beijerinck var. *vulgaris* SAG 211-11b and was used in this study. *C. vulgaris* was cultured in 3N-BBM media (CCAP, 2024) with the following composition: 750 mg/L $NaNO_3$, 25 mg/L $CaCl_2 \cdot 2H_2O$, 75 mg/L $MgSO_4 \cdot 7H_2O$, 75 mg/L K_2HPO_4, 175 mg/L KH_2PO_4, 25 mg/L NaCl, 0.8 mg/L Fe(III)EDTA and 1 mL trace metal

solution; 3.7 g/L $Na_2EDTA \cdot 2H_2O$, 246 mg/L $MnSO_4 \cdot 4H_2O$, 30 mg/L $ZnCl_2$, 12 mg/L $CoCl_2 \cdot 6H_2O$ and 24 mg/L $(NH_4)_6Mo_7O_{24} \cdot 7H_2O$, 168 mg/L $NaHCO_3$. In addition, Tris-hydroxymethyl 1M (pH 7.5) was added as pH buffer of 3N-BBM media.

The preculture was conducted in continuous mode in a 1-L glass Roux bottle photobioreactor with an optical path length of 5 cm and an effective volume of 500 mL. Aeration is conducted at 1 L min^{-1} (2 vvm), and the cultivation bottle was irradiated at 100 µmol m^{-2} s^{-1}. The media feeding rate was controlled with a peristaltic pump (Watson pump 323S) at 100 mL d^{-1} resulting in the dilution rate of 0.2 d^{-1}, so that the cell state of late log-growth phase is constantly maintained. During the steady-state, the optical density (OD) was maintained between 0.8 and 1.8 (Fig. 2), and the pH fluctuated within the range of 8 to 9 (Fig. 3). The cells at the steady state were used for the experiment.

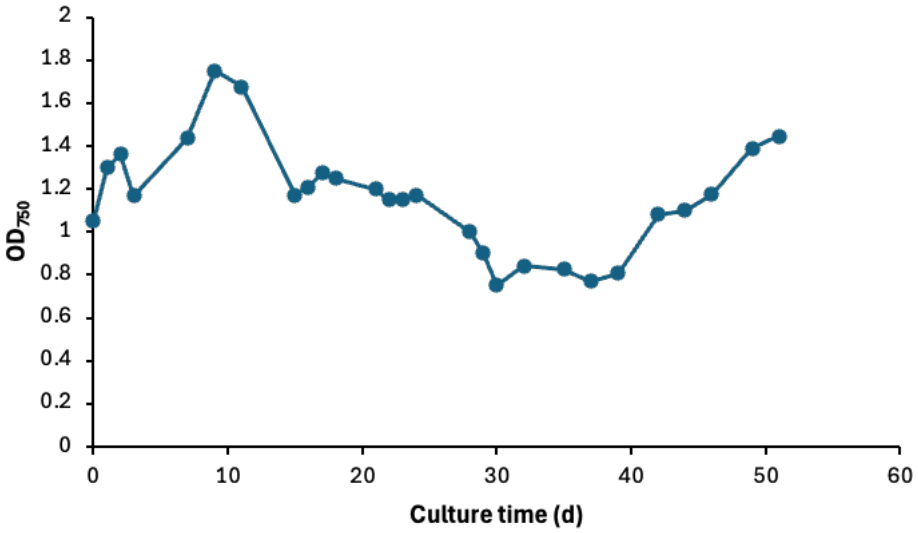

Fig. 2. Time course of OD_{750} of *C. vulgaris* at continuous preculture

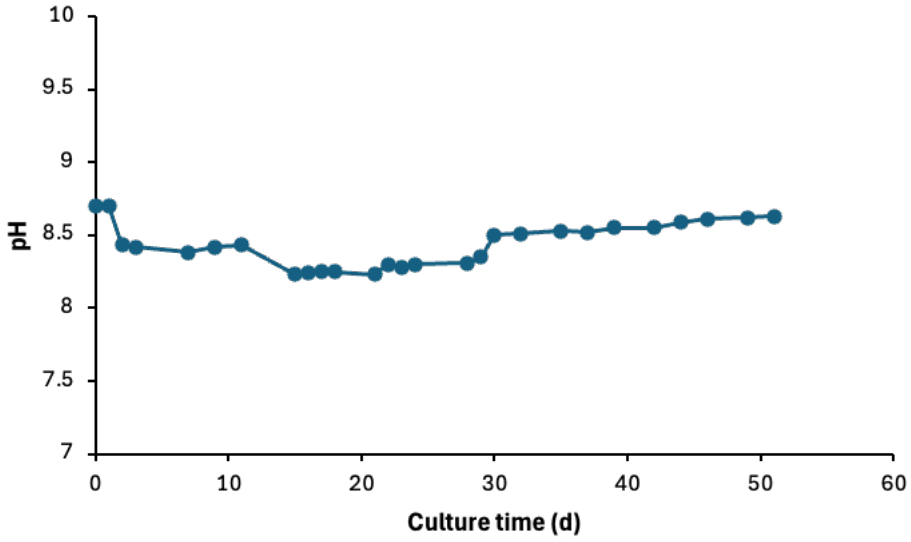

Fig. 3. Time course of pH of *C. vulgaris* at pre-continuous culture

In the experiment, the concentration of $MgSO_4 \cdot 7H_2O$ in the 3N-BBM medium was reduced from 75 mg/L to 7.5 mg/L in order to prevent magnesium precipitation with the addition of high-concentration NH_4Cl. In addition, to prevent carbon limitation during the microalgal growth, $NaHCO_3$ was added at a concentration of 672 mg/L. The pH of the medium was carefully adjusted to 8.3 to maintain the concentration of free ammonia at levels known to inhibit microalgal activity.

3.2. Experiment 1: Characterization of OJIP curve under NH_3, heat, and high light stress

Chlorella vulgaris was exposed to five ammonia concentrations (N0, N1, N2, N3 and N4; Table 1) in five 120 mL serum bottles, under triplicate conditions. Ammonia was added to the culture media in the form of NH_4Cl, and the concentration of free ammonia (NH_3) was calculated based on pH, temperature, and ionic strength. Since the acid dissociation constant (pKa), which governs the equilibrium between NH_4^+ and NH_3, is temperature-dependent, the resulting NH_3 concentrations from N0 to N4 varied across experimental conditions (Table 1). *Chlorella vulgaris* was inoculated from pre-culture to 120 mL serum bottles to be OD_{750} of 0.1 as initial concentration with fresh modified 3N-BBM medium. Following inoculation, these cultures in serum bottles were dark-adapted for 10 min, and then ammonia was added to each serum bottle. Measurement of pH, fluorescent analysis, and OD_{750} were performed after adding ammonia. After 5 hours of incubation, the same measurement was performed.

Table 1. Free ammonia concentration (mM) of N0 to N4 at each experimental condition

	N0	N1	N2	N3	N4
25°C	0.000	0.645	1.210	2.724	4.222
35°C	0.000	0.957	1.923	3.759	6.008
40°C	0.000	1.054	2.013	3.615	6.645
High light	0.000	0.526	1.063	2.130	4.402

High light: 500 µmol m^{-2} s^{-1} environmental

To expose the cells to heat and high light stress, various temperature and light intensity conditions were adopted for the 5-h incubation of the algal cells. As a control condition, 25°C with 100 µmol photons m^{-2} s^{-1} was used. For the heat stress, 35°C and 40°C was conducted. As for the high light stress, 500 µmol photons m^{-2} s^{-1} was used while maintaining the control temperature of 25°C. At 35, 40°C and high light conditions, except 25°C, values of pH, OJIP, and OD_{750} were measured only after 5 hours, assuming the same cell conditions at the start of the experiments throughout all conditions because of the steady state preculture.

From the obtained fluorescent transient data, three fluorescent parameters, Fv/Fm, V_K, and V_L, were calculated to investigate their response towards each stress. These parameters were selected because of their frequent appearance in the study of photosystem inhibition (Wang et al., 2011; Cai et al., 2023; Zhou et al., 2015).

3.3. Experiment 2: Effects of saturation pulse intensity on chlorophyll fluorescence

Three intensities of saturation pulse (SP1, SP2, and SP3 corresponding to 575, 1405, and 2700 µmol m^{-2} s^{-1}, respectively) were used for the measurement of OJIP fluorescent transient to assess the effects on the fluorescence values. For this purpose, two distinct sets of measurements were conducted as follows.

First, the samples from Experiment 1 were used to analyze the effect of saturation pulse intensity, so that its effect on the distinction of different photosystem stresses can be simultaneously investigated. The measurement was conducted after 5 hours of incubation in the respective conditions.

Second, the combined effects of saturation pulse intensity and optical density (OD) on the fluorescent signals were investigated, so as to provide the basis for the development of standardized procedures for fluorescence data acquisition and interpretation. OJIP transients were measured at seven biomass concentrations ranging from 0.04 to 2.48 OD_{750} (Table 2) using three different saturation pulse intensities (SP1, SP2, and SP3). To obtain the high-density biomass, the precultured cells were centrifuged at 2400 rpm for 10 minutes. The resulting pellets were resuspended and diluted using fresh 3N-BBM medium of the same composition as the preculture to achieve the desired concentrations. Following a 10-minute dark adaptation period, OJIP measurements were conducted in triplicate. Under high optical density (OD) and high saturation pulse intensities, fluorescence signals reached saturation and were excluded for the analysis (Table 3).

Table 2. Optical density at each OD condition

	OD1	OD2	OD3	OD4	OD5	OD6	OD7
OD (750 nm)	0.04	0.08	0.16	0.33	0.60	1.22	2.48

Table 3. Relationship between OD condition at each saturation pulse intensity (L1, L2 an L3)

		L1	L2	L3
	SPI / OD (750 nm)	575	1405	2700
OD1	0.04	✓	✓	✓
OD2Times	0.08	✓	✓	✓
OD4Times	0.16	✓	✓	✓
OD8Times	0.33	✓	✓	Saturated
OD16Times	0.60	✓	Saturated	Saturated
OD32Times	1.22	✓	Saturated	Saturated
OD64Times	2.48	✓	Saturated	Saturated

✓ = Acceptable

3.4. Analysis and calculations

Fluorescent measurements, namely OJIP and LC2 protocols, were conducted with AquaPen-C (AP110-C, PSI, Czech Republic). For evaluation of microalgal biomass, optical

density at 750 nm (OD_{750}) was measured using a spectrophotometer (SHIMADZU UV-2550). For the measurement of pH, a pH meter (CRISON basic 20+) was utilized.

Specific growth rate (μ; d^{-1}) was calculated using OD_{750} at Time 0 and Time 5 using the following formula.

$$\mu = \frac{\ln(X_2) - \ln(X_1)}{t_2 - t_1}$$

where X_i is the biomass concentration (OD_{750}) at time t_i (d).

3.4.1. Fluorescent parameter calculations and data quality assurance

V_L and V_K are the relative variable fluorescence at 150 µs and 300 µs and were calculated using Equations (1) and (2), respectively. These two values are commonly used as indicators of stress conditions such as salinity, drought, and chemical stress (Wang et al., 2011, Koller et al., 2013, Cai et al., 1917).

$$V_L = (F_{150\mu s} - Fo)/ (F_M - F_o) \quad (1)$$

$$V_K = (F_{300\mu s} - Fo)/ (F_M - F_o) \quad (2)$$

where F_o = fluorescence at 40 µs, F_M = maximum value under saturating illumination. In addition, to visualize changes in the K and L bands, the double-normalized SP1 fluorescence values between F_O (40 µs) and F_J (2 ms) and between F_O and F_K (300 µs) were calculated for each condition, and the values for the control condition were subtracted from those for the treatment conditions (e.g., ammonia-stressed). As the time to reach both L-band and K-band peaks shortened, specific time points were defined for parameter extraction. In SP2, the fluorescence intensity at 130 µs (F_{130}) was used to calculate V_{130}. In SP3, fluorescence intensities at 70 µs (F_{70}) and 520 µs (F_{520}) were used to derive V_{70} and V_{520}, respectively. These values were incorporated as OJIP parameters in the multivariable analysis. Other values were defined using OJIP parameters as determined by the AquaPen (Table 4).

Table 4. Modified OJIP parameters from the instructions of AquaPen-C

Abbreviation	Explanation
Bckg	Background
F_0	$F_0 = F_{50\mu s}$, fluorescence intensity at 50 µs
F_j	F_j = fluorescence intensity at J-step (at 2 ms)
F_i	F_i = fluorescence intensity at I-step (at 30 ms)
F_m	F_m = maximal fluorescence intensity
F_v	$F_v = F_m - F_0$ (maximal variable fluorescence)
F_L	F_L = fluorescence intensity at L-band (at 150 µs)
F_K	F_K = fluorescence intensity at K-step (at 300 µs)
Flast *	Flast = fluorescence intensity at 2 s
F70 *	F70 = fluorescence intensity at 70 µs
F130 *	F70 = fluorescence intensity at 130 µs
F520 *	F520 = fluorescence intensity at 520 µs
V_j	$V_j = (F_j - F_0) / (F_m - F_0)$
V_i	$V_i = (F_i - F_0) / (F_m - F_0)$
V_L	$V_L = (F_L - F_0) / (F_m - F_0)$
V_K	$V_K = (F_K - F_0) / (F_m - F_0)$
Vlast *	Vlast = (Flast - F_0) / (F_m - F_0)
V_{70} *	$V_{70} = (F_{70} - F_0) / (F_m - F_0)$
V_{130} *	$V_{130} = (F_{130} - F_0) / (F_m - F_0)$
V_{520} *	$V_{520} = (F_{520} - F_0) / (F_m - F_0)$
F_m / F_0	-
F_v / F_0	-
F_v / F_m	-
V_i/V_j	-
Mo (or dV/dt)$_0$	$Mo = TR_0/RC - ET_0/RC = 4 \times (F_{300} - F_0) / (F_m - F_0)$
S_m	S_m = Area / (F_m - F_0) (multiple turn-over)
S_s	S_s = the smallest S_m turn-over (single turn-over)
N	$N = S_m \cdot Mo \cdot (1 / V_j)$, turn-over number QA
Phi_P_0	Phi_P_0 = 1 - (F_0 / F_m) (or F_v / F_m)
Phi_Pav	Phi_Pav = Phi_P_0 (S_m / t_m) ; t_m = time to reach F_m (in ms)
ABS / RC	$ABS / RC = Mo \cdot (1 / V_j) \cdot (1 / Phi\_P_0)$
TR_0 / RC	$TR_0 / RC = Mo \cdot (1 / V_j)$
ET_0 / RC	$ET_0 / RC = Mo \cdot (1 / V_j) \cdot Psi_0$
P time *	Times ; Fluorescence value showed maximum

To assure the quality of fluorescent data, each fluorescent measurement was evaluated with a set of criteria as follows to exclude irregular or noisy measurement. First, double-normalizedormSP1 (with F_M and F_O) standard deviation of the fluorescent values between 250 and 350 µs (K-band) exceeding 5 were removed.

3.4.2. Multivariable analysis

Lasso regression analysis was performed in this study to identify the variables contributing to the classification of ammonia levels. Lasso (Least Absolute Shrinkage and Selection Operator) regression is a linear regression method that employs SP1 regularization to both prevent overfitting and perform automatic variable selection by shrinking the coefficients of less relevant variables to zero. The same dataset was used for both the training and validation phases in the analysis.

The overall analysis was divided into three major sample groups: the temperature set (Temperature set), which combined three temperature conditions; the light set (Light set), which included both normal and high light conditions; and the temperature-light combined set (Combined set), which combined three temperature and one high light conditions. To assess the inhibitory effects of ammonia under high temperature and high light stress, to evaluate the variables common to both conditions, and to investigate the influence of saturation pulses, each variable group was evaluated under the following conditions: (1) Temperature set at each saturation pulse condition (SP1, SP2, and SP3), (2) Light set at each saturation pulse condition, (3) Combined set at each saturation pulse condition (4) the combination of all three saturation pulse conditions (SP1, SP2, and SP3) for each set, (5) the combination of two saturation pulse conditions (SP1 and SP3) for each set, and (6). Model performance was evaluated using several statistical indicators, including Mean Squared Error (MSE), the coefficient of determination (R^2) for predictive accuracy, the Pearson correlation coefficient (r), the number of variables selected by the model, and the identities of the selected variables.

4. Results

4.1. Growth of C. vulgaris in this experiment

The specific growth rate ranged between 1.3 d^{-1} to negative values (Fig. 4). At 25°C and 35°C, the specific growth rate increased from N0 to N1, followed by a gradual decline toward N4 with increasing NH_3 concentrations. While NH_3 concentrations were higher in 35°C than in 25°C owing to the pKa change with high temperature, the growth remained relatively high even at N4 condition. Under the high light condition, no growth was observed even at no or low NH_3 conditions (N0-N2). In the high temperature (40°C) and high light conditions, biomass decreased compared to Time 0 in N3 and N4 treatments.

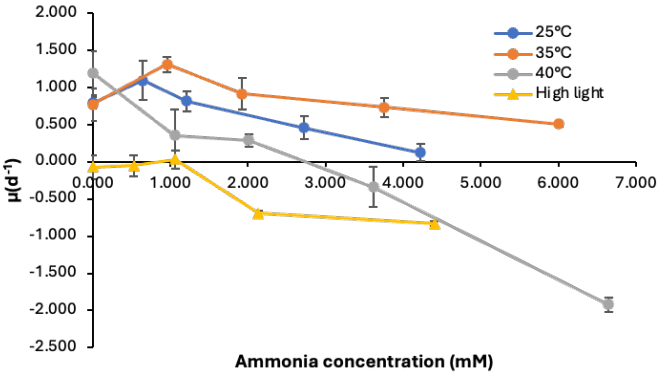

Fig. 4. Specific growth rate (μ) at each experimental condition

4.2. Detection of photosystem stress through fluorescence

4.2.1. NH_3 stress

In the treatment groups N1 to N4, increasing ammonia concentrations resulted in a decline in Fv/Fm values, indicating that the photosynthetic activity of *C. vulgaris* was inhibited by ammonia toxicity (Table 2). A few minutes after ammonia addition (Time 0), clear changes in the fluorescence values and OJIP fluorescence transients were observed in all treatment groups compared to the non-treated condition (N0) (Fig. 5A and C), demonstrating that ammonia-induced stress could be detected at a very early stage using chlorophyll fluorescence

measurements. At Time 0, an ammonia-concentration-dependent increase in O peak was observed from N0 to N3. On the other hand, in N4, a further increase in O peak was not observed, but instead, P peak decreased, and the I peak was no longer observed (Fig. 5A and C).

At Time 5, the I and P peaks progressively declined from N0 to N4 (Fig. 5B and D). In the N4 treatment, the transient curve showed a different shape compared with other treatment conditions; the J peak even exceeded the P peak (Fig. 5D). In the relative fluorescence (Fig. 5D), substantial concentration-dependent increase of the slope before the J peak was observed

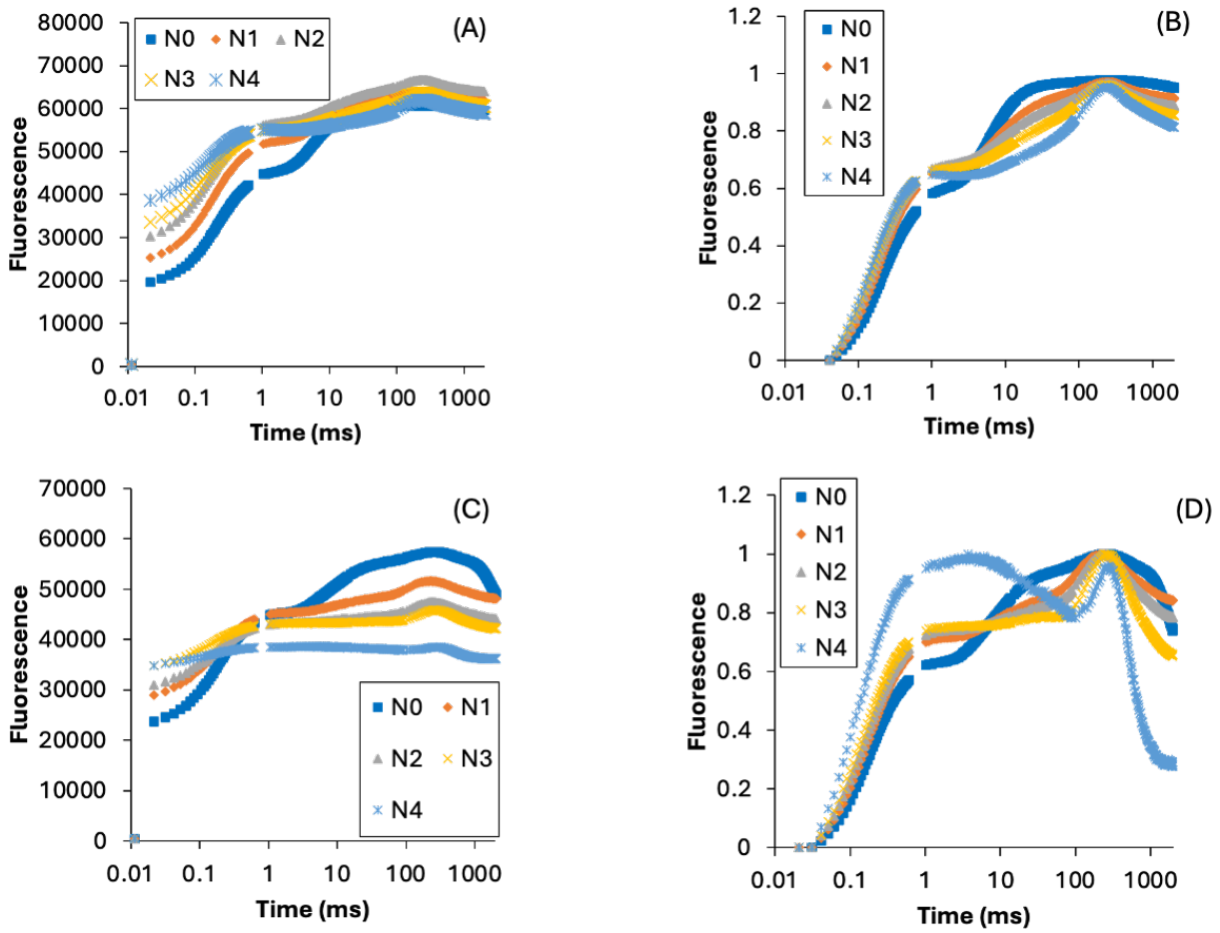

Fig. 5. OJIP curve at 25ºC; OJIP fluorescence at Time 0 (A and C) and Time 5 (B and D), OJIP. fluorescence curve (A and C), normalized OJIP fluorescence curve (B and D)

4.2.2. High temperature stress

At 25 °C and 35 °C, the Fv/Fm values remained comparable for each NH_3 condition (Table 2). However, a substantial decrease in Fv/Fm was observed at 40 °C, particularly under ammonia-treated conditions (N1–N4) where values approached zero or were completely undetectable. The fluorescent data obtained in these conditions did not satisfy the required standard for further analysis owing to the large variation. The Fv/Fm of the N0 condition at high heat stress with 40°C was reduced to 0.20±0.02, which was less than half of that at 25°C

and 35°C (Table 5).

Table 5. Fv/Fm of each ammonia concentration at each experimental condition

	N0	N1	N2	N3	N4
Time0	0.66 ± 0.00	0.58 ± 0.00	0.52 ± 0.00	0.44 ± 0.00	0.35 ± 0.03
25°C Time5	0.56 ± 0.01	0.41 ± 0.02	0.32 ± 0.02	0.22 ± 0.01	0.08 ± 0.03
35°C Time5	0.56 ± 0.01	0.44 ± 0.01	0.37 ± 0.02	0.23 ± 0.00	0.01 ± 0.00
40°C Time5	0.20 ± 0.02	0.00	0.00	0.00	0.000
High light Time5	0.21 ± 0.01	0.14 ± 0.00	0.12 ± 0.01	0.05 ± 0.01	0.02 ± 0.00

Between 25 °C and 35 °C, no substantial alterations were observed in the shape of the OJIP curves, although J, I, and P peaks were slightly high at 25 °C (Fig. 6A). In contrast, under 40 °C conditions, the OJIP curves exhibited obvious change: the J peak became elevated and closely approached the intensity of the P peak (Fig. 6B).

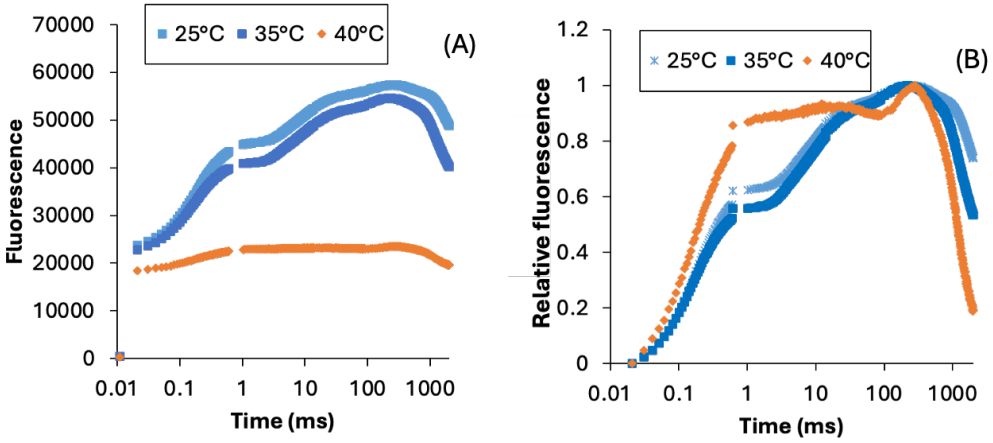

Fig. 6. OJIP curve of N0 at three temperature conditions: (A) OJIP fluorescence curve, (B) normalized OJIP fluorescence curve.

4.2.3. High environmental light stress

At high light (500 µmol m^{-2} s^{-1}) conditions, Fv/Fm without NH_3 (N0) was reduced to 0.22±0.02, which was close to the value of highly inhibited 40°C (Table 4). The Fv/Fm of N1 and N2 remained relatively high despite the combined high-light and ammonia stress, while that of N3 and N4 were low. The fluorescent data of N3 and N4 did not satisfy the criteria and thus were not used for further analysis.

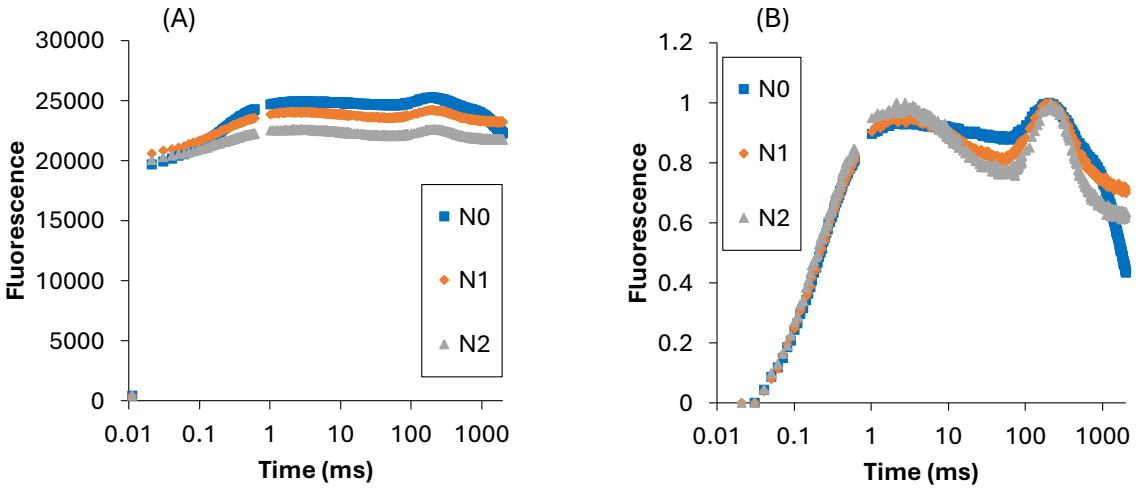

Fig. 7. OJIP curve under high light condition; (A) OJIP fluorescence curve, (B) normalized OJIP fluorescence curve

The fluorescence intensity near the I peak was lower in the ammonia-treated groups compared to the control. Under all three conditions, including without N0, the J peak exhibited close values to the P peak (Fig. 7. A and B).

4.2.4. Comparison of the fluorescence and growth among different types of stress

SP2 OJIP curves of three stresses, namely heat (40 ºC N0), high light (500 µmol m^{-2} s^{-1} N0), and high ammonia (25 ºC N4), were compared with that of the control condition (25°C N0) (Fig. 8A and B). As a result, increases of fluorescence before the I peak were observed in all stress condition. The I peak was not observed in high light and ammonia conditions, and relative fluorescence value gradually decreased from the J peak to approximately 100 ms.

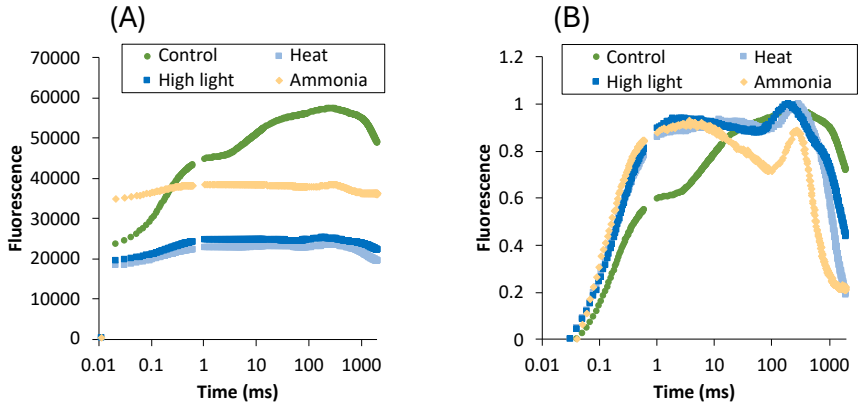

Fig. 8. (A) OJIP curve and (B) Normalized OJIP curve under stress conditions; Control (25ºC N0), Heat (40ºC N0), High light (500 µmol m^{-2} s^{-1} N0), Ammonia (25ºC N4)

The value of Fv/Fm decreased in an ammonia-dependent manner. However, it also declined under high temperature and high light conditions, resulting in a low correlation with ammonia concentration ($R^2 = 0.156$) (Fig. 9A).

Both V_L and V_K values increased in an ammonia-dependent manner under all conditions except for the high-light condition. Among the three temperature conditions (25 ºC Time 0, 25 ºC Time 5 and 35 ºC), a similar increasing trend was observed. Although the values of V_L and V_K also shifted upwards with rising temperature, relatively high correlation coefficients of 0.68 for V_L and 0.64 for V_K were obtained by using all the data (Fig. 9B and C).

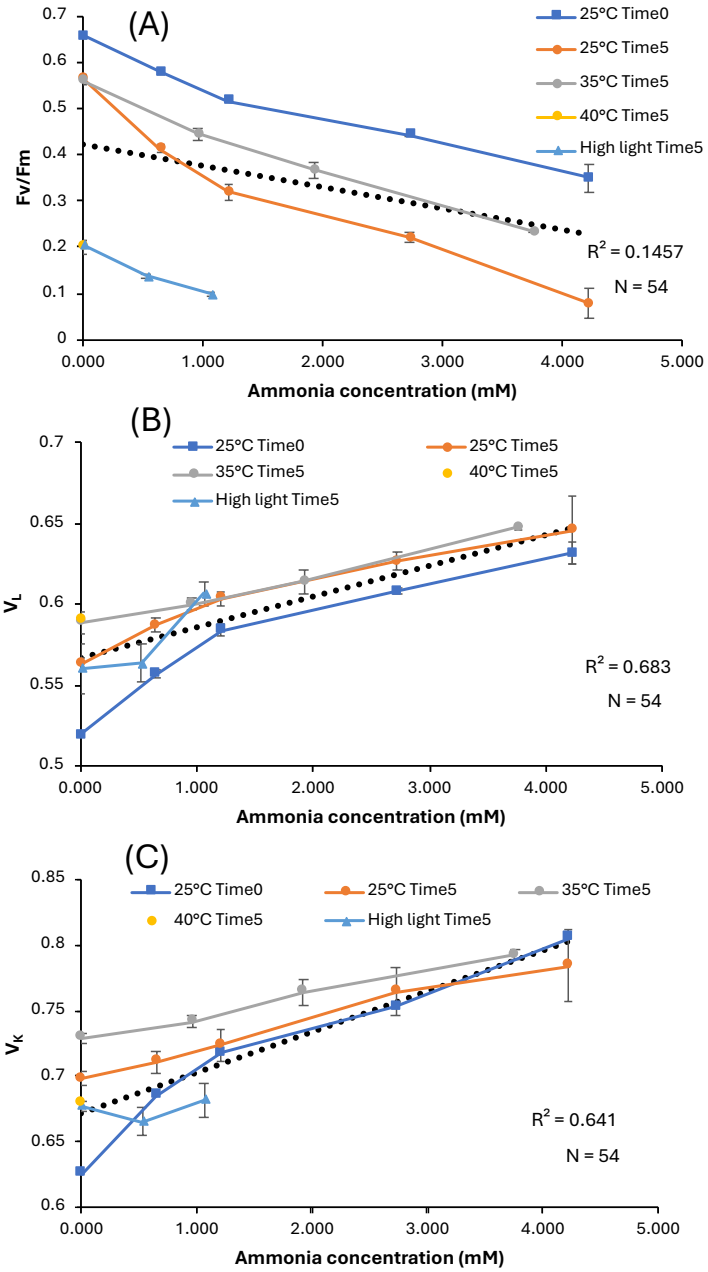

Fig. 9. (A) Fv/Fm, (B) Specific growth rate (μ), (C) V_L, and (D) $V_K$of each ammonia concentration at different experimental conditions

4.3. Effects of saturation pulse intensity

4.3.1. Effects of saturation pulse intensity on OJIP curve

In the SP1 OJIP curves corresponding to the three levels of saturation pulse, the first step of fluorescence rise (before the J peak) was elevated with increasing saturation pulse intensity (Fig. 10). When the fluorescent values were compared among different pulse intensities, a characteristic peak of L to K bands were observed. While the L and K bands corresponded well with ammonia concentration (Fig. 11A, B and C, 12A, B and C), increase in the saturation pulse intensity also induced L and K band increase (Fig. 10A, B and C, 11A, B and C). Furthermore, the fluorescent maxima shifted leftward from approximately 300 µs in SP1 to 120 µs in SP2 (Fig. 10B and 11B). The maxima further divided into two in SP3 (2700 µmol m^{-2} s^{-1}) at around 70 µs and 520 µs depending on the ammonia concentration (Fig. 10C).

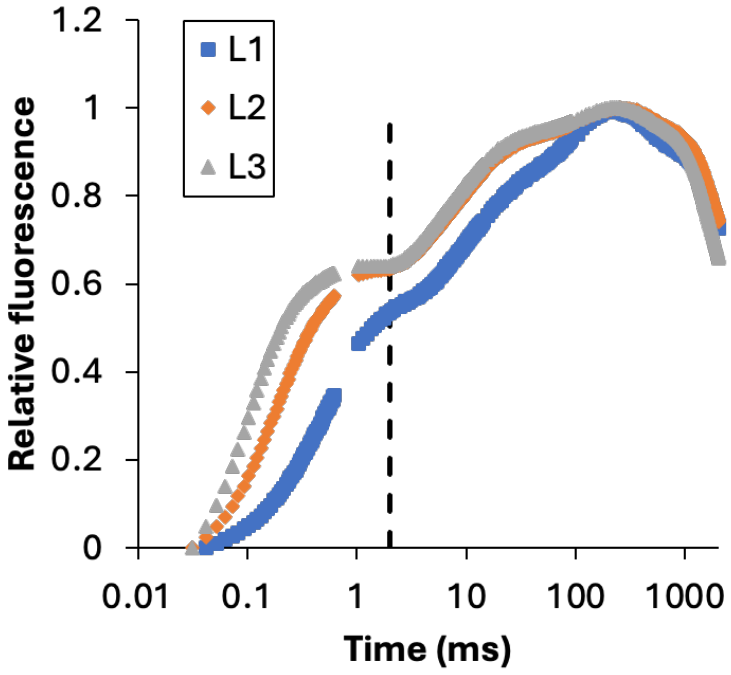

Fig. 10. Normalized OJIP curve of 25ºC of L1, L2 and L3 at N0 condition

On the other hand, noisy variation of the fluorescent values decreased with higher saturation pulse intensity, as apparent in the O-J SP1 values (Fig. 11A, B and C). The reduction of variation was even more apparent in the L-band characterization (Fig. 12), where the difference among NH_3 levels is obscure with low saturation pulse intensity SP1 (Fig. 12A), while it is clear in higher intensity SP2 and SP3 (Fig. 12B and C).

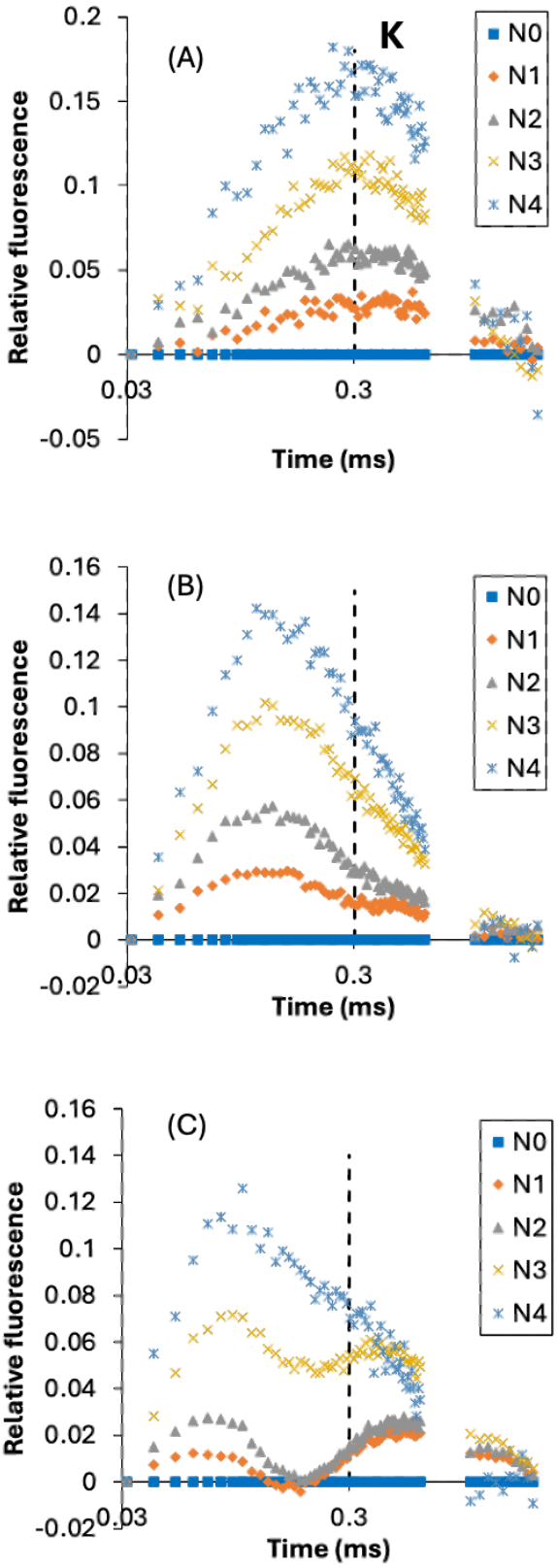

Fig. 11. Normalized K-band of 25ºC of L1 (A), L2 (B) and L3 (C)

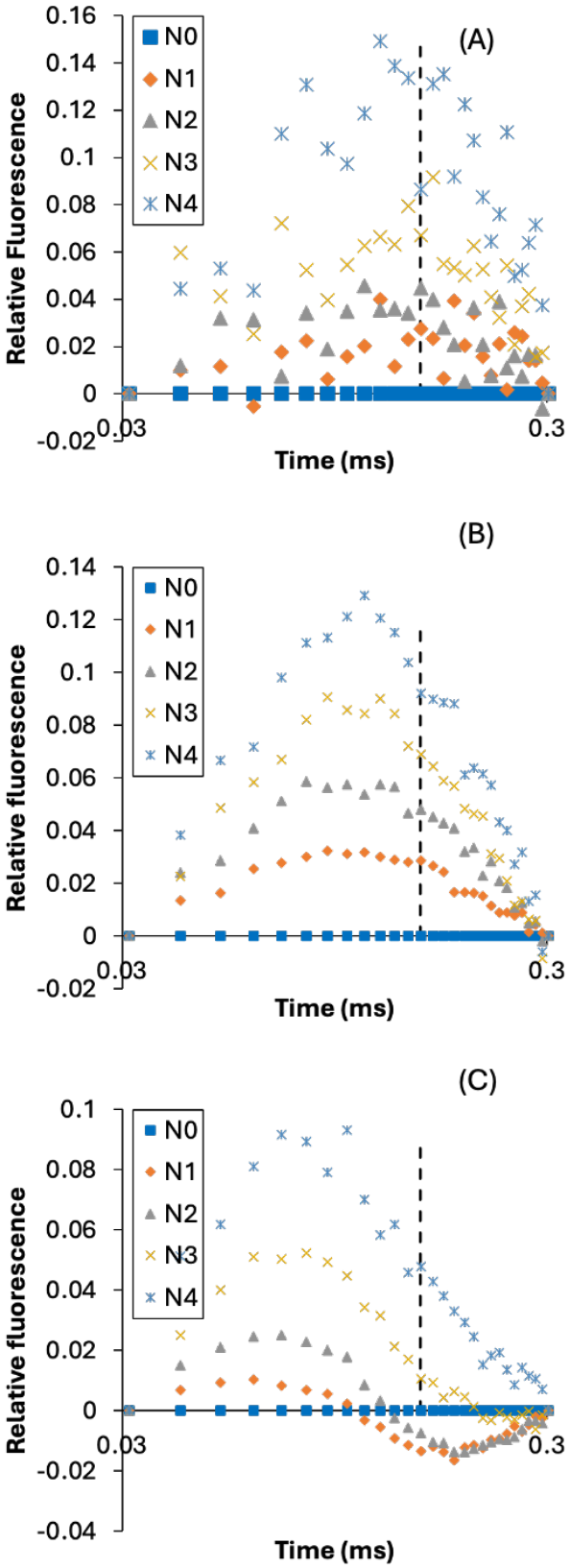

Fig. 12. Normalized L-band of 25ºC of L1 (A), L2 (B) and L3 (C)

4.3.2. Relationship between saturation pulse intensity and optical density

To evaluate the effect of increasing saturation pulse intensity and OD, the K bands were analyzed using the data of the lowest pulse intensity and OD (OD1-SP1) as the control (Fig. 13). As a result, the saturation pulse intensity exhibited stronger influence on the change of fluorescence than the OD did. While the change of relative fluorescence caused by OD ranged within 0.1, that by the pulse intensity reached as high as 0.5. Similarly, the peak position shift was pulse intensity dependent than OD. Still, higher OD induced the opposite effect of the higher saturation pulse intensity; namely reduction of K band and the peak shift towards right (Fig. 13A, B and C). The effect of the OD was more apparent with higher saturation pulse intensity. Thus, at SP1, there was negligible difference among OD1 through OD4, while clear differences were observed in SP2 and SP3.

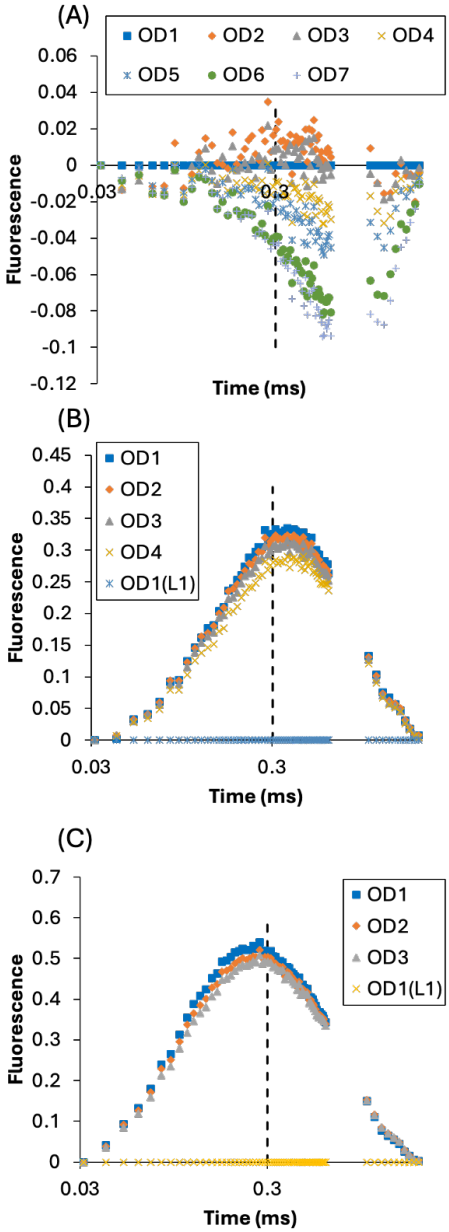

Fig. 13. K-band of different OD at each SP condition; (A) 575, (B)1405, and (C)2700 µmol m^{-2} s^{-1}

4.4. Selected variables and detection accuracy of multivariable analysis

4.4.1. Temperature data set

At Temperature set of each saturation pulse intensity, Lasso regression selected 6, 6 and 3 parameters as variables for SP1, SP2 and SP3 conditions, respectively (Table. 6). The prediction accuracy, correlation coefficient, and mean squared error (MSE) for conditions SP1, SP2, and SP3 were 0.88, 0.95, and 0.22 (SP1); 0.87, 0.94, and 0.23 (SP2); and 0.91, 0.96, and 0.18 (SP3), respectively (Fig. 14A, D and G). Among the three conditions, SP3 exhibited the highest prediction accuracy and correlation coefficient, as well as the lowest MSE. TRo/RC, Vlast, V_L, ABS/RC, Phi_Pav, V_K, Mo, P time, V_{520} and V_{70} were selected as variables. While TRo/RC, Vlast, V_L and V_K were selected in both SP1 and SP2 conditions, the three variables V_{520}, V_{70} and Phi_Pav were selected in SP3 condition.

4.4.2. High light data set

For each level of saturation pulse intensity (SP1, SP2, and SP3), the Lasso regression model selected 6, 4, and 3 variables, respectively. The corresponding values of prediction accuracy, correlation coefficient, and mean squared error (MSE) were 0.82, 0.91, and 0.30 for SP1; 0.79, 0.89, and 0.33 for SP2; and 0.83, 0.92, and 0.28 for SP3 (Fig. 14B, E and H). Among the three settings, SP1 demonstrated the best model performance, showing the highest prediction accuracy and correlation along with the lowest MSE. The selected variables included TRo/RC, V_K/Vj, Phi_Pav, Vlast, V_L, V_K, N, V_{520}, Sm, V_{70}, and ABS/RC. Of these, TRo/RC and V_L were common to both SP1 and SP2, while V_{520}, V_{70} and Sm were selected under the SP3 condition.

4.4.3. Combined temperature and light conditions data set

At each saturation pulse intensity (SP1, SP2, and SP3), Lasso regression identified 4, 5, and 3 variables, respectively. The associated prediction accuracy, correlation coefficient, and mean squared error (MSE) were 0.83, 0.92, and 0.29 for SP1; 0.84, 0.92, and 0.27 for SP2; and 0.84, 0.92, and 0.27 for SP3 (Fig. 15C, F and I). Among these conditions, the SP1 setting exhibited the most favorable model performance, with the highest prediction accuracy and the lowest MSE. The selected variables reflected the same values in the Temperature set and Light set analyses, TRo/RC, Vlast, and V_L were commonly selected in both SP1 and SP2, while V_{520}, Sm and V_{70} were specific to the SP3 condition.

4.4.4. All saturation pulse combinations

For the Temperature set, Light set, and Combined set, the prediction accuracy, correlation coefficient, and mean squared error (MSE) were 0.91, 0.96, and 0.15; 0.88, 0.94, and 0.19; and 0.90, 0.96, and 0.16, respectively (Fig. 15A, C and E). All conditions demonstrated comparable or higher performance relative to each corresponding set (T, L and Combined set). A total of 9, 7, and 8 variables were selected for the Temperature set, Light set, and Combined set, respectively.

4.4.5. SP1&SP3 combination

The Temperature set, Light set, and Combined set yielded prediction accuracies, correlation coefficients, and mean squared errors (MSE) of 0.92, 0.96, and 0.16; 0.88, 0.94, and 0.20; and 0.91, 0.96, and 0.16, respectively (Fig. 15B, D, and F). These results indicate that all models exhibited comparable or superior performance compared to their respective individual sets. The number of variables selected by Lasso regression was 7 for the Temperature set, 7 for

the Light set, and 9 for the Combined set.

4.4.6. The Temperature set analysis using the Light set as teaching data.

Using the Light set, data from the Temperature set excluding 25°C (i.e., 35°C and 40°C) were analyzed. The prediction accuracy, correlation coefficient, and mean squared error (MSE) were 0.41, 0.78, and 0.96, respectively (Fig. 16). These results showed that the Light set was capable of reasonably estimating the ammonia stress levels even under high-temperature conditions.

4.4.7. Effects of saturation pulse on estimation of ammonia concentration

The data obtained from OJIP measurement by SP1 was used as teaching data, and the data obtained from OJIP measurement by SP3 was predicted. In addition to that, data of SP3 was also used as teaching data, and SP1 was predicted. The results showed negative value of R-squared. Prediction accuracy showed low value compared to other Lasso regression analysis. In the case that teaching data was SP1, predicted ammonia concentration was high compared to actual value. On the other hand, predicted ammonia concentration was low when the SP3 data was used as teaching data (Fig. 17A, B).

Table 6. The variables selected by multivariable analysis

	SP1	SP2	SP3	AllSP	SP1&3
Temperature set	6	6	3	9	7
Light set	6	4	3	7	7
Combined set	4	5	3	8	9

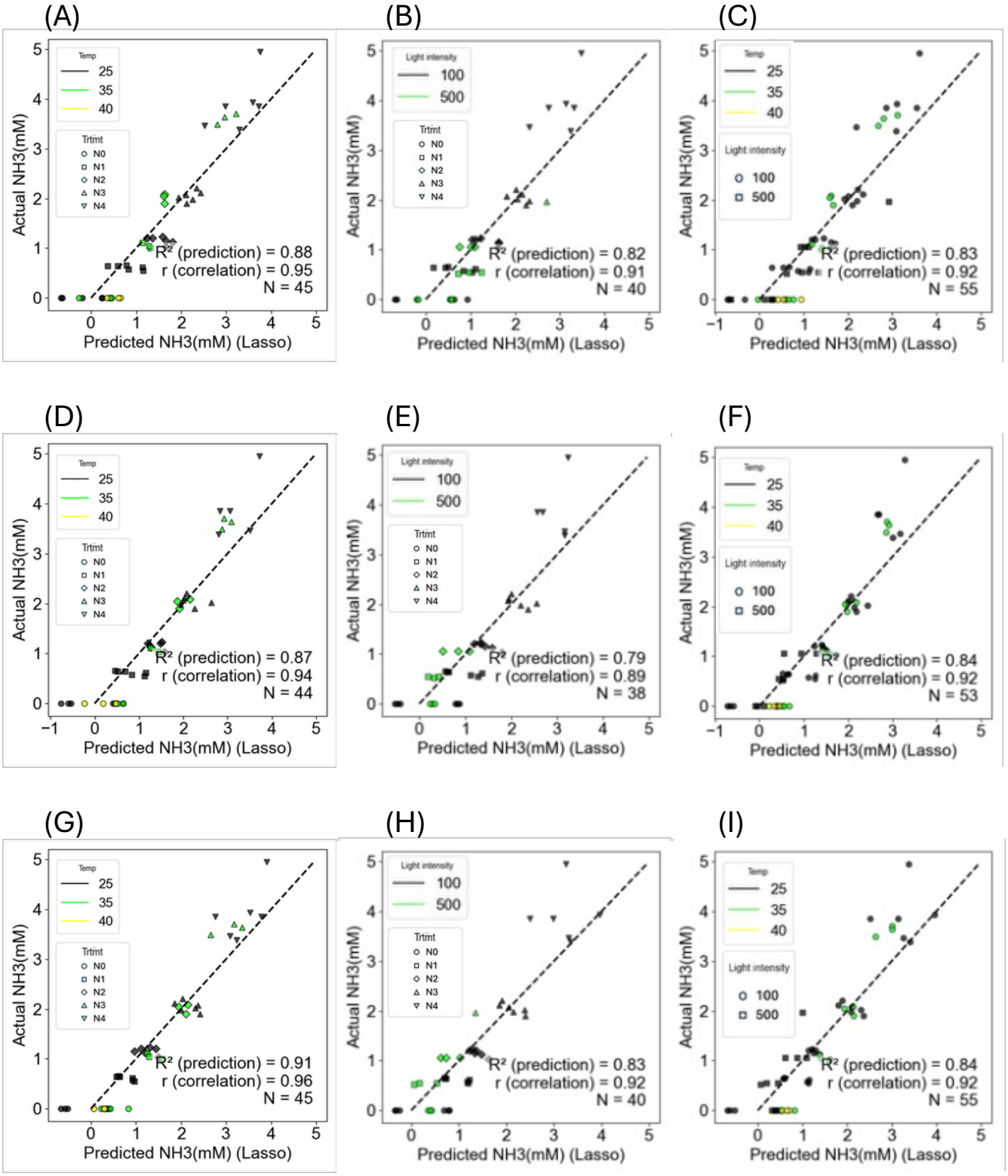

Fig. 14. Results of Lasso regression; Temperature data set (A, D and G), Light data set (B, E and H) and combined both conditions (C, F and I) at saturation pulse SP1 (A, B and C), SP2 (D, E and F) and SP3 (G, H and I)

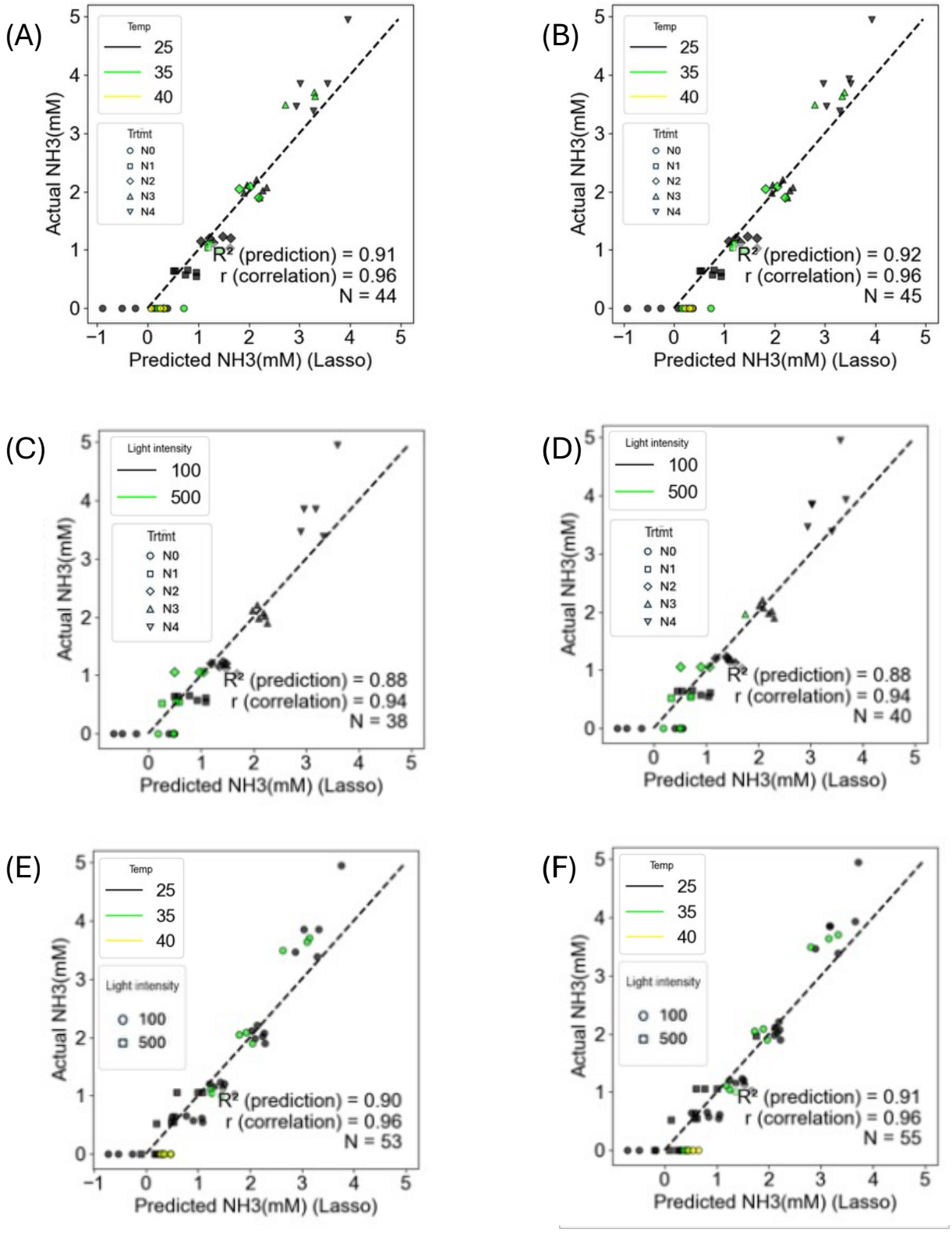

Fig. 15. Results of Lasso regression; Temperature data set (A and B), Light data set (C and D) and combined both conditions (E and F) at all saturation pulse (A, C and E) and combined SP1 and SP3 (B, D and F)

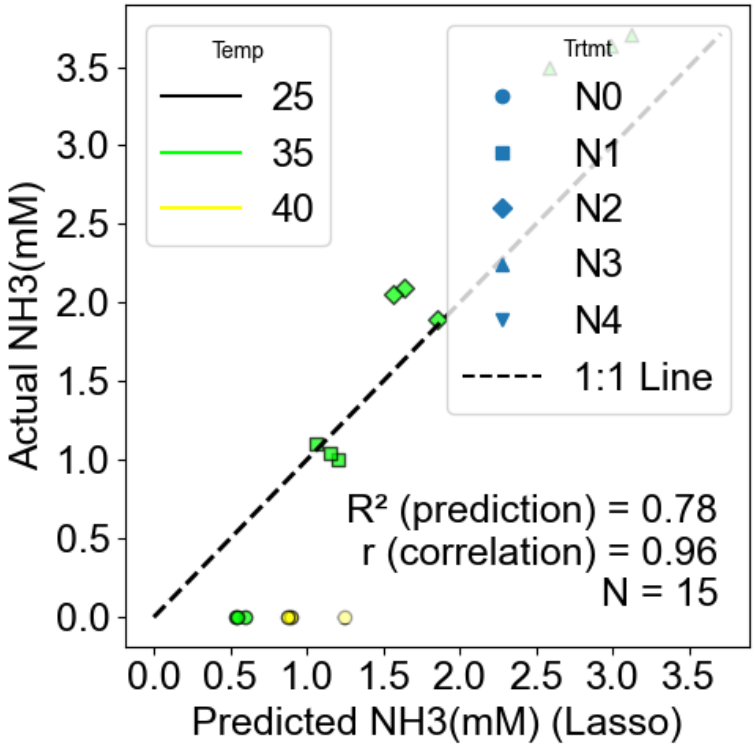

Fig. 16. Results of Lasso regression; Temperature set analysis using the Light set as teaching data.

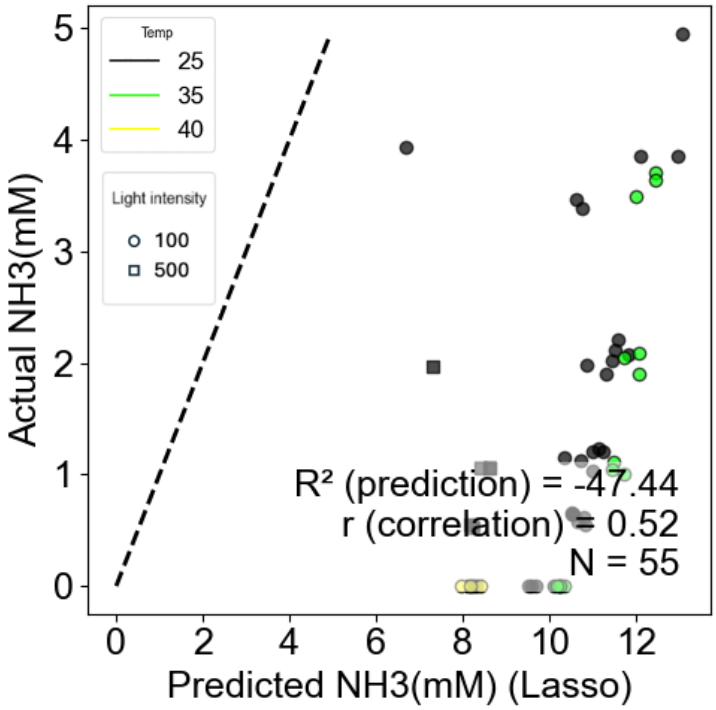

Fig. 17. Results of Lasso regression; teaching data is SP1 and predicted data is SP3

5. Discussion

5.1. Difference of chlorophyll fluorescence between three stresses (NH3, heat and high light)

The rapid response of fluorescence and OJIP curves after addition of ammonia (Table 3) is consistent with findings by Markou et al. (2016) and Kishi et al. (unpublished). OJIP curve can be useful as a tool to monitor algal ammonia inhibition as it can respond quickly to the change of the culture environment.

Ammonia is known to disrupt the manganese cluster of the oxygen-evolving complex (OEC), impairing oxygen evolution (Oyala et al., 2015). The overall reduction in fluorescent intensity (Fig. 5C) indicated that ammonia stress inhibited not only the OEC but also other components of photosystem II (PSII). The overall reduction of fluorescent intensity agreed with the results reported by Markou et al. (2016). The rise before the J peak in relative fluorescence reflects the appearance of the K-band, which is widely recognized as a diagnostic marker of OEC damage (Strasser et al., 2004). Given that this increase accelerates with rising ammonia concentrations, it suggests that the fluorescence characteristics before the J peak may contribute to the early detection of ammonia-induced inhibition in photosynthetic systems.

Compared to the relatively low heat stress observed at 25 °C and 35 °C, exposure to 40 °C resulted in a pronounced photosynthetic inhibition, indicating that the photosynthetic system is highly sensitive to extreme heat stress at this temperature. These results strongly indicate that exposure to 40 °C causes severe inhibition of photosynthetic activity, overriding any additional stress effects induced by ammonia. In fact, under 40 °C conditions, the OJIP curves exhibited pronounced distortion (Fig. 6B). The J peak of 40 °C became elevated and closely approached the intensity of the P peak, suggesting severe disruption of electron transport through PSII.

The increase in the J peak under ammonia, heat, and light stress has been reported in previous studies (Markou et al., 2016; Jedmowski and Brüggemann, 2015; Jin et al., 2017), and our experimental results are consistent with these findings. Comparison of the OJIP curves showed that under high ammonia conditions, the O peak value was elevated compared to both the control condition (25 °C) and the high light condition. However, under heat stress, a similar O peak was observed (Fig. 8A). Moreover, since raw fluorescence intensity is largely influenced by microalgal biomass concentration and the intensity of the saturation pulse, it is difficult to use as a reference in actual monitoring. In the normalized OJIP curves, an increase in the J peak and similar trends leading to the P peak were observed, suggesting that specific detection of ammonia using OJIP curves alone may be challenging (Fig. 8B).

As such environmental stresses can simultaneously occur in outdoor wastewater treatment and algal cultivation facilities, a way to precisely distinguish the cause of inhibition is required. Although Fv/Fm is commonly used as an indicator for detecting photosynthetic inhibition (Makarova et al., 1998; Zhou et al.; 2015; Lin et al., 2022), it was found to drastically decrease under high-temperature and high-light stress conditions. For instance, the value of the N3 condition at Time 5 under 25 °C was comparable to that of the N0 condition under high light intensity (Table 2). This suggests that while a correlation between Fv/Fm and ammonia concentration was observed within each controlled condition, the overlapping effects of multiple stresses may hinder the detection of ammonia-specific inhibition in field environments. In contrast, V_L and V_K appeared to be less sensitive to high temperature or photoinhibition.

Despite a slight increase in their values with rising temperature, these parameters exhibited relatively strong correlations with ammonia concentration across various conditions (Fig. 9B and C). Elevated V_L and V_K values are indicative of the appearance of the L-band and K-band, which are known markers of structural and functional disruptions in PSII.

The K-band and L-band have previously been reported to appear under specific stress conditions, such as heat or nitrogen deficiency for the K-band, and high temperature or salt stress for the L-band (Strasser et al., 2004; Chen et al., 2016; Wang et al., 2023). The present results demonstrate that ammonia toxicity can also induce both bands. Furthermore, their appearance showed a strong correlation with increasing ammonia concentration, in a range larger than the heat and photoinhibition, suggesting that the parameters derived from fluorescence transients may serve as sensitive indicators of ammonia-induced PSII inhibition.

5.2. Effects of saturation pulse on chlorophyll fluorescence

The increase in saturation pulse intensity elevated the fluorescence before the J peak, namely K and L bands (Fig. 10) most likely because of the accelerated reduction rate of Q_A by the stronger light energy. Not only the peak height but also shifts of the peak time was observed with increased pulse intensity (Fig. 11A, B and C, 12A, B and C). These phenomena can be problematic for the selective detection of NH_3, because the useful parameters for NH_3 detection, namely V_K and V_L, can be altered by the saturation pulse intensity, which can vary among the fluorometer. Actually, the model that treated the data obtained from SP1 as teaching data overestimated predicted ammonia concentration of SP3 data (Fig. 17). Furthermore, if cell self-shading within the measurement cuvette alters the effective saturation pulse intensity, the standardization of ammonia monitoring is further complicated.

Increasing the saturation pulse caused the peaks of the K band and L band to shift to the left. However, this leftward shift became less pronounced as the OD increased. As discussed later, the peak positions of the K and L bands significantly influence the prediction of ammonia concentrations. Therefore, standardization of OD and saturation pulse intensity is essential for accurate measurement of ammonia concentration. Furthermore, increasing the saturation pulse intensity improved the detection of the K and L bands. This improvement is likely due to the enhancement of fluorescence intensity, which facilitates the differentiation of conditions. Thus, it is considered important to maintain a saturation pulse intensity above a certain threshold.

However, it was suggested that OD has much less effect than the saturation pulse intensity irradiated from the fluorometer (Fig. 13). For example, at a low saturation pulse (SP1), the 4-times increase of OD from 0.04 to 0.16 (OD1 to OD4) had negligible effect on the K-band. On the other hand, less than 3-time increase of pulse intensity (575 to 1405 μmol photons m^{-2} s^{-1}) induced drastic effect (Fig. 13A and B). Furthermore, the leftward shift of the K-band due to increased saturation pulse intensity also had a more pronounced effect than the influence of microalgal biomass concentration (OD_{750}) especially at high saturation pulse. Based on these findings, the same fluorescent parameter could be used for a good range of OD if saturation pulse intensity is fixed. Nevertheless, self-shading still exerted some influence, as the K-band amplitude decreased with increasing OD especially at high saturation pulse intensities. In addition, another problematic phenomenon occurred was the range limit of fluorometer. In the SP2 condition, where the K-band was relatively well-defined, the maximum detectable OD was 0.33. However, actual biomass concentrations in wastewater treatment facilities are typically higher. Under conditions of both high saturation pulse and high OD, fluorescence intensity

reached saturation, resulting in measurement failure. Therefore, further improvements in instrumentation or method are necessary to enable detection under higher biomass conditions.

Concluding this section, saturation pulse intensity affected on OJIP parameters more than OD of microalgae. It suggests that saturation pulse intensity should be constant when OJIP is used as a tool of ammonia monitoring.

5.3. Multivariable analysis

The Lasso multiple regression analysis was able to create models that can estimate the NH_3 concentration at prediction accuracy of up to $R^2 = 0.92$ (Fig. 14 and 15) with reduced number of variables (3–11; Table 5) despite the variable temperature and light conditions. This result indicates that OJIP fluorescent data contains enough information to selectively and quantitatively detect NH_3 stress under the existence of heat and light stress. The prediction accuracy was much higher than that obtained solely by V_L and V_K ($R^2 = 0.68$ and 0.64, respectively; Fig. 9B and C) owing to the combination of parameters.

The higher predictive performance observed from the Temperature set compared to the Light set (Fig. 14G and H) may be attributed to the limited number of samples under the latter. Analysis across both temperature and light datasets revealed considerable variability in the predicted values for the N0 condition, which overlapped with those of the N1 condition. This suggests that the heat and light stress on PSII components deteriorates the prediction accuracy at a low-level NH3 (N0 to N1), while that has less effect at higher NH_3 levels. Furthermore, despite the exclusion of highly variable samples based on a predefined criterion, predicted N4 values remained lower than the actual values. This shift of N4 indicates that severe ammonia inhibition may not be accurately captured, most likely because of the limited capable range of PSII response to a severe stress.

Among the variables selected for both the Temperature set and Light set in SP1 and SP2 conditions, V_L, TR_o/RC and Vlast were consistently included. TR_o/RC, which represents the trapped energy flux per reaction center (RC), is known to be a reliable indicator under stress conditions such as high temperature and salinity (Wassie et al., 2019; Guo et al., 2019), and its increase with rising ammonia concentration suggests that RCs are inhibited by ammonia. Vlast, derived from the final fluorescence intensity (Flast) at 2000 ms, was effective with a low saturation pulse intensity (SP1) and showed a decreasing trend with increasing ammonia levels. V_L, which demonstrated a relatively strong correlation with ammonia concentration ($R^2 = 0.68$), was also effective in SP1 analysis.

While SP1 and SP2 primarily included parameters known to be associated with other environmental stresses, SP3 consistently selected V_{70} and V_{520} across all data sets. This highlights the critical role of K-band peaks measured at high saturation pulse intensity in detecting ammonia toxicity. An increase in saturation light intensity did not always contribute to an improvement in accuracy. However, combining data from different saturation light intensities led to enhanced accuracy (Fig. 15A, C, E), albeit with an increased number of variables. When parameters from all three saturation pulse levels (SP1, SP2, and SP3) were included, improvements were observed in prediction accuracy, correlation, and MSE across all data sets compared to the analysis conducted at individual saturation pulse intensity. However, variables selected from SP1 and SP3 dominated the model, while those from SP2 were comparably a few. This suggested that combining parameters from both low (SP1) and high (SP3) saturation pulse intensities can sufficiently enhance ammonia prediction performance, achieving comparable or superior accuracy.

In the combined analysis of SP1 and SP3, five identical variables (V_{520} (SP3), TRo/RC (SP1 and SP3), Phi-Pav (SP1), and Vlast (SP1)) were selected across both the Temperature set and the Light set. Consequently, when predicting the Temperature set (excluding 25°C to avoid overlap between teaching and predicting data) using the Light set as the model-teaching dataset, relatively high prediction accuracy was achieved. This suggests that a single model can be used to predict NH3 level, distinguishing it from heat and light stress, probably because these five variables are more strongly correlated with ammonia stress than with temperature or light stress. While relatively low ammonia stress levels, such as N1 and N2, were predicted accurately, the predicted values for N0 were overestimated by approximately 0.5 to 1.0 mM compared to the estimation value. This indicates that when temperature or light causes inhibitory effects similar to those of ammonia stress, the model may misinterpret them as ammonia stress, and its accuracy is deteriorated at low NH_3 levels. Increase in the teaching dataset may improve model refinement to avoid such issues in the future, as better prediction accuracy was observed when both Temperature and Light sets were used for model teaching (Fig. 15F).

The model that treated the data obtained from SP1 as teaching data overestimated predicted ammonia concentration of SP3 data, and the opposite model underestimated predicted ammonia concentration. Chlorophyll fluorescence intensity is enhanced by increasing saturation pulse. Additionally, some parameters, such as V_L and V_K, exhibited a positive correlation with ammonia concentration. It is considered that the high chlorophyll fluorescence intensity of the data obtained from SP3 was misrecognized by the model SP1 used as teaching data as high ammonia inhibition. This result showed that this model must be used under same saturation pulse intensity measurement.

5.4. Implication

In this study, Lasso regression analysis model was found to be able to estimate ammonia concentration by OJIP measurement under high light and high temperature stress conditions. This indicates that OJIP measurement has the possibility of being used as a monitoring tool for ammonia concentration in a wastewater treatment reactor. On the other hand, there are still challenges. Firstly, ammonia prediction of this model has a range that functions effectively. High ammonia concentration conditions were underestimated through this study. Furthermore, effects of high light, high temperature, and ammonia stress on OJIP parameter are somewhat similar, although the effects were relatively more strongly observed with ammonia stress. The relative fluctuation of prediction was large at low ammonia concentration of nearly 0 mM mainly owing to the effects of light and temperature stress. Therefore, in the case that very sensitive monitoring is needed, this model should be combined with other monitoring tools that can measure very low ammonia concentrations. Secondly, it was found that saturation pulse intensity elevates important OJIP parameters. Inaccurate prediction was observed when a model created by a different saturation pulse intensity was used. This result suggests that the saturation pulse intensity needs to be carefully adjusted essential for the prediction of ammonia toxicity. On the other hand, if saturation pulse intensity is accurately adjusted, combination of different intensities was found to enhance the prediction accuracy under high light and high temperature stress.

6. Conclusion

While qualitative OJIP curves did not allow for distinction between stress types such

as temperature, high light intensity, and ammonia inhibition, quantitative parameters such as V_L and V_K showed a relatively high correlation with ammonia concentration. Furthermore, multivariable analysis enabled a more accurate prediction of ammonia levels. An increase in saturation pulse intensity accelerated the emergence of the K-band peak, and the resulting parameters (V_{70} and V_{520}) contributed significantly to the prediction accuracy. These findings suggest that enhanced saturation pulse intensity improves the precision of ammonia concentration estimation. However, as saturation pulse intensity increases, the measurable range of biomass concentration without fluorescence signal saturation narrows. Therefore, further instrument and/or method development and standardization of saturation pulse settings are essential to ensure accurate and robust application of this method in practice.

Reference

Bates, H., Zavafer, A., Szabó, M., Ralph, P. J., 2019. A guide to Open-JIP, a low-cost open-source chlorophyll fluorometer. Photosynth. Res. 142, 361-368. https://doi.org/10.1007/s11120-019-00673-2

Cai, Y., Qi, Y., Zhu, S. Q., Nian, H., He, G. Q., Xu, N., 2023. Effects of Cadmium Stress on Photosynthetic Apparatus of Tobacco. Appl. Ecol. Environ. Res. 21, 1917-1929. https://doi.org/10.15666/aeer/2103_19171929

Chen, S., Yang, J., Zhang, M., Strasser, R. J., Qiang, S., 2016. Classification and characteristics of heat tolerance in Ageratina adenophora populations using fast chlorophyll a fluorescence rise O-J-I-P. Environ. Exp. Bot. 122, 126-140. https://doi.org/10.1016/j.envexpbot.2015.09.011

Collos, Y. and Harrison, P. J., 2014. Acclimation and toxicity of high ammonium concentrations to unicellular algae. Mar. Pollut. Bull. 80, 8-23. http://dx.doi.org/10.1016/j.marpolbul.2014.01.006

Culture Collection of Algae and Protozoa (CCAP), 2025. 3N-BBM+V (Bold Basal Medium with 3-fold Nitrogen and Vitamins; modified). Available at: https://www.ccap.ac.uk/wp-content/uploads/MR_3N_BBM_V.pdf (accessed 12 July 2025).

Duarte, B., Gameiro, C., Utkin, A. B., Matos, A. R., Caçador, I., Fonseca, V., Cabrita, M. T., 2021. A multivariate approach to chlorophyll a fluorescence data for trace element ecotoxicological trials using a model marine diatom. *Estuar. Coast. Shelf Sci.* 250, 107170. https://doi.org/10.1016/j.ecss.2021.107170

Gan, T., Yin, G., Zhao, N., Tan, X., Wang, Y., Sheng, R., Ye, Z., 2023. A new sensitive response index for detecting water toxicity based on microalgal fluorescence kinetics. J. Appl. Phycol. 35, 2219-2239. https://doi.org/10.1007/s10811-023-03066-0

Georgieva, K., Tsonev, T., Velikova, V., Yordanov, I., 2000. Photosynthetic activity during high temperature treatment of pea plants. J. Plant Physiol. 157, 169-176. https://doi.org/10.1016/S0176-1617(00)80187-X

Gentili, F.G. & Fick, J. (2017) Algal cultivation in urban wastewater: an efficient way to reduce pharmaceutical pollutants. Journal of Applied Phy-cology, 29, 255–262. https://doi.org/10.1007/s10811-016-0950-0.

Guisse, B., Srivastava, A., Strasser, R. J., 1995. The polyphasic rise of the chlorophyll a fluorescence (O-K-J-I-P) in heat stressed leaves. Arch. Sci. Genève 48, 1-14. https://doi.org/10.5169/SEALS-740252

Guo, Y. Y., Nie, H. S., Yu, H. Y., Kong, D. S., Wu, J. Y., 2019. Effect of salt stress on the growth and photosystem II photochemical characteristics of *Lycium ruthenicum* Murr. seedlings. *Photosynthetica* 57, 564–571. https://doi.org/10.32615/ps.2019.068

Jedmowski, C., Brüggemann, W., 2015. Imaging of fast chlorophyll fluorescence induction curve (OJIP) parameters, applied in a screening study with wild barley (*Hordeum spontaneum*) genotypes under heat stress. *J. Photochem. Photobiol. B* 151, 153–160. https://doi.org/10.1016/j.jphotobiol.2015.07.020

Jin, L., Che, X., Zhang, Z., Li, Y., Gao, H., Zhao, S., 2017. The mechanisms by which phenanthrene affects the photosynthetic apparatus of cucumber leaves. *Chemosphere* 168, 1498–1505. https://doi.org/10.1016/j.chemosphere.2016.12.002

Kalaji, H.M., Schansker, G., Ladle, R.J., Goltsev, V., Bosa, K., Allakhverdiev, S.I., Brestic, M., Bussotti, F., Calatayud, A., Dąbrowski, P., Elsheery, N.I., Ferroni, L., Guidi, L., Hogewoning, S.W., Jajoo, A., Misra, A.N., Nebauer, S.G., Pancaldi, S., Penella, C., Poli, D., Pollastrini, M., Romanowska-Duda, Z.B., Rutkowska, B., Serôdio, J., Suresh, K., Szulc, W., Tambussi, E., Yanniccari, M., Zivcak, M., 2014. Frequently asked questions about in vivo chlorophyll fluorescence: Practical issues. Photosynth. Res. 122, 121–158. https://doi.org/10.1007/s11120-014-0024-6

Koller, S., Holland, V., Brüggemann, W., 2013. Effects of drought stress on the evergreen Quercus ilex L., the deciduous Q. robur L. and their hybrid Q. × turneri Willd. Photosynthetica 51, 574-582. https://doi.org/10.1007/s11099-013-0058-6

Lee, S. A., Lee, N., Oh, H. M., Ahn, C. Y., 2021. Stepwise treatment of undiluted raw piggery wastewater, using three microalgal species adapted to high ammonia. Chemosphere 263, 127934. https://doi.org/10.1016/j.chemosphere.2020.127934

Lin, L., Chan, G. Y. S., Jiang, B. L., Lan, C. Y., 2007. Use of ammoniacal nitrogen tolerant microalgae in landfill leachate treatment. Waste Manage. 27, 1376-1382. https://doi.org/10.1016/j.wasman.2006.09.001

Lin, S. Y., Chen, P. A., Zhuang, B. W., 2022. The Stomatal Conductance and Fv/Fm as the Indicators of Stress Tolerance of Avocado Seedlings under Short-Term Waterlogging. *Agronomy* 12, 1–11. https://doi.org/10.3390/agronomy12051084

Lincoln, E. P., Koopman, B., Bagnall, L. O., Nordstedt, R. A., 1986. Aquatic system for fuel and feed production from livestock wastes. *J. Agric. Eng. Res.* 33, 159–169. https://doi.org/10.1016/S0021-8634(86)80046-4

Makarova, V., Kazimirko, Y., Krendeleva, T., Kukarskikh, G., Lavrukhina, O., Pogosyan, S., Yakovleva, O., 1998. Fv/Fm as a Stress Indicator for Woody Plants from Urban-Ecosystem. *Photosynthesis: Mechanisms and Effects*, 4065–4068. https://doi.org/10.1007/978-94-011-3953-3_943

Markou, G., Depraetere, O., Muylaert, K., 2016. Effect of ammonia on the photosynthetic activity of Arthrospira and Chlorella: A study on chlorophyll fluorescence and electron transport. Algal Res. 16, 449–457. https://doi.org/10.1016/j.algal.2016.03.039

Marchão, L., da Silva, T. L., Gouveia, L., Reis, A., 2018. Microalgae-mediated brewery wastewater treatment: effect of dilution rate on nutrient removal rates, biomass biochemical composition, and cell physiology. J. Appl. Phycol. 30, 1583-1595. https://doi.org/10.1007/s10811-017-1374-1

Sawayama, S., Minowa, T., Dote, Y., Yokoyama S., 1992. Growth of the hydrocarbon-rich microalga *Botryococcus braunii* in secondarily treated sewage. Appl Microbiol Biotechnol 38, 135–138. https://doi.org/10.1007/BF00169433

Strasser, B. J., 1997. Donor side capacity of Photosystem II probed by chlorophyll a fluorescence transients. Photosynth. Res. 52, 147-155. https://doi.org/10.1023/A:1005896029778

Strasser, R.J., M. Tsimilli-Michael, A. Srivastava (2004). Analysis of the Chlorophyll a Fluorescence Transient, In G.C. Papageorgiou, Govindjee, eds., Springer Netherlands, 321–362. https://link.springer.com/chapter/10.1007/978-1-4020-3218-9_12

Sutherland, D. L., 2022. Improving microalgal tolerance to high ammonia with simple organic carbon addition for more effective wastewater treatment. J. Water Process Eng. 47, 102667. https://doi.org/10.1016/j.jwpe.2022.102667

Teoh, M. L., Phang, S. M., Chu, W. L., 2013. Response of Antarctic, temperate, and tropical microalgae to temperature stress. J. Appl. Phycol. 25, 285-297. https://doi.org/10.1007/s10811-012-9863-8

Thach, L. B., Shapcott, A., Schmidt, S., Critchley, C., 2007. The OJIP fast fluorescence rise characterizes *Graptophyllum* species and their stress responses. *Photosynth. Res.* 94, 423–436. https://doi.org/10.1007/s11120-007-9207-8

Wang, G., Chen, L., Hao, Z., Li, X., Liu, Y., 2011. Effects of salinity stress on the photosynthesis of Wolffia arrhiza as probed by the OJIP test. Fresen. Environ. Bull. 20, 432-438.

Wang, X. S., Wang, J., Yin, J. C., Li, J. H., 2023. Comparison of the physiological factors in ion accumulation and photosynthetic electron transport between legumes Medicago truncatula and Medicago sativa under salt stress. Plant Soil 484, 473-486. https://doi.org/10.1007/s11104-022-05811-9

Wassie, M., Zhang, W., Zhang, Q., Ji, K., Chen, L., 2019 Effect of Heat Stress on Growth and Physiological Traits of Alfalfa (Medicago sativa L.) and a Comprehensive Evaluation for Heat Tolerance. Agronomy. 9, 597. https://doi.org/10.3390/agronomy9100597

Zushi, K., Kajiwara, S., Matsuzoe, N., 2012. Chlorophyll a fluorescence OJIP transient as a tool to characterize and evaluate response to heat and chilling stress in tomato leaf and fruit. Sci. Hortic. 148, 39-46. https://doi.org/10.1016/j.scienta.2012.09.022

Zhou, R., Yu, X., Kjær, K. H., Rosenqvist, E., Ottosen, C. O., Wu, Z., 2015. Screening and validation of tomato genotypes under heat stress using Fv/Fm to reveal the physiological mechanism of heat tolerance. *Environ. Exp. Bot.* 118, 1–11. https://doi.org/10.1016/j.envexpbot.2015.05.006